



ELSEVIER

Contents lists available at ScienceDirect

## Journal of Magnetism and Magnetic Materials

journal homepage: [www.elsevier.com/locate/jmmm](http://www.elsevier.com/locate/jmmm)

# Hydrodynamic and magnetic fractionation of superparamagnetic nanoparticles for magnetic particle imaging

Norbert Löwa<sup>a,\*</sup>, Patrick Knappe<sup>b</sup>, Frank Wiekhorst<sup>a</sup>, Dietmar Eberbeck<sup>a</sup>,  
Andreas F. Thünemann<sup>b</sup>, Lutz Trahms<sup>a</sup>

<sup>a</sup> Physikalisch-Technische Bundesanstalt, Abbestr. 2-12, 10587 Berlin, Germany

<sup>b</sup> Bundesanstalt für Materialforschung und -prüfung, Unter den Eichen 87, 12205 Berlin, Germany



## ARTICLE INFO

## Article history:

Received 30 June 2014

Accepted 16 August 2014

Available online 30 August 2014

## Keywords:

Superparamagnetic nanoparticles  
Asymmetric flow field–flow fractionation  
Magnetic particle spectroscopy  
Magnetorelaxometry  
Magnetic separation  
Magnetic particle imaging  
Resovist<sup>®</sup>

## ABSTRACT

Resovist<sup>®</sup> originally developed as a clinical liver contrast agent for Magnetic Resonance Imaging exhibits also an outstanding performance as a tracer in Magnetic Particle Imaging (MPI). In order to study the physical mechanism of the high MPI performance of Resovist<sup>®</sup>, we applied asymmetric flow field–flow fractionation (A4F) and static magnetic fractionation (SMF) to separate Resovist<sup>®</sup> into a set of fractions with defined size classes. As A4F based on an elution method separates MNP according to their hydrodynamic size, SMF fractionates a particle distribution by its magnetic moment. The obtained fractions of both separation techniques were then magnetically characterized by magnetorelaxometry measurements to extract the corresponding effective magnetic anisotropy and hydrodynamic size distribution parameters. Additionally, the MPI performance of each fraction was assessed using magnetic particle spectroscopy. With both separation techniques fractions (normalized to their iron amount) an MPI signal gain of a factor of two could be obtained, even though the distribution of effective anisotropy and hydrodynamic size were significantly different. Relating these findings to the results from magnetic characterization allows for a better understanding of the underlying mechanisms of MPI performance of Resovist<sup>®</sup>. This knowledge may help to improve the design of novel MPI tracers and development of separation methods.

© 2014 Elsevier B.V. All rights reserved.

## 1. Introduction

The properties of magnetic nanoparticles (MNP) are strongly dependent on their size, which often exhibit a broad distribution. To this end, in many applications only a small proportion of particles contribute to the desired magnetic effect. This applies in particular to the novel imaging modality magnetic particle imaging (MPI) which is based on the nonlinear magnetization properties of MNP, the so called tracer and allows for background-free imaging of MNP distributions in living organisms with high spatial and excellent temporal resolution [1]. Besides the development of applicable MPI scanner systems and methods for image reconstruction, the optimization of MNP properties are of prerequisite for MPI image quality at present [2]. This is due to the fact that both, sensitivity and spatial resolution of MPI are strongly influenced by the magnetic characteristics of the tracer,

particularly the MNP core size and anisotropic contributions, i.e. shape and crystal structure [3].

So far, Resovist<sup>®</sup> has been mostly used as MPI tracer as it exhibits surprisingly high signal performance. Furthermore, it has the advantage to be clinically approved for in-vivo MR imaging and is therefore widely tested. Nevertheless, Resovist<sup>®</sup> is far away from being optimized for MPI. Studies revealed that this sample exhibits a bimodal size distribution, consisting of small primary particles, some of which form stable aggregates (multi-core particles) [4]. Therefore, the isolation of this large sized particle population responsible for the high MPI signal is of great interest. Several attempts were made to separate Resovist<sup>®</sup> magnetically [5,6] and characterize the obtained fractions with regard to MPI performance [7–9]. Furthermore, asymmetric flow field–flow fractionations (A4F) were performed to gain insight into the distribution of hydrodynamic sizes of Resovist<sup>®</sup> as this method gently produces fractions of narrow hydrodynamic size distribution and permits highly reproducible and accurate size evaluations [4,10,11]. In addition, A4F was also shown to be suitable for the preparation of fractions with different magnetic properties [12]. In the present work, we compare the impact of both fractionation

\* Corresponding author. Tel.: +493034817736.

E-mail address: [norbert.loewa@ptb.de](mailto:norbert.loewa@ptb.de) (N. Löwa).

methods on MPI signal enhancement of Resovist<sup>®</sup> with respect to structural differences. To estimate the distribution of hydrodynamic sizes and to evaluate the separation process samples were measured by dynamic light scattering (DLS) and magnetorelaxometry (MRX) in liquid state. In addition, MRX measurements on samples with immobilized MNP were performed to gain information about the distribution of effective magnetic core sizes and anisotropy energies  $E_A$  which determine the responsiveness of MNP to the MPI excitation field. This is of essential interest as Ferguson et al. [13] experimentally found an MPI tracer size optimum at 20 nm. Conversely, simulations from Weizenecker et al., taking into account the anisotropy contributions, showed that larger MNP are expected to perform better in MPI [3]. They found 25 nm to 30 nm particles at  $E_A/k_B T = 1.7$  and 1.2, respectively, to be responsible for Resovist<sup>®</sup>'s superior MPI performance.

For the assessment of MPI performance of the individual fractions we used a magnetic particle spectrometer (MPS), which can be considered as a zero-dimensional MPI scanner.

## 2. Materials and methods

### 2.1. Samples

The separations were performed on DDM128 (Meito Sangyo, Japan) an aqueous suspension of iron oxide nanoparticles coated with carboxydextran which is a precursor of the clinical formulation Resovist<sup>®</sup> [14]. Suspension material was first centrifuged gently at 3000 g for 1 min to remove highly aggregated particles and the supernatant with a final iron concentration of 411 mmol/L was denoted as sample of initial state.

Deionized water containing 0.2% (v/v) FL70 detergent (Fisher Sci., USA) was used as carrier liquid for A4F. Triton X-100 diluted in water to a final concentration of 0.05% (v/v) was used as a wetting agent to prepare the SMF column. For the elution of the particles carboxydextran solution (0.25 g/mL) was used to prevent

aggregation of the fractions due to detachment of the stabilizing coating. All liquids were degassed prior to use.

For magnetic measurements (MRX, MPS) a sample volume of 30  $\mu$ L sample volume was filled in PCR tubes (fast reaction tube with cap, Appl. Biosystems, USA). Additionally, MNP were immobilized by adding mannitol solution (7% w/v) to the sample before freeze-drying for the purpose to preserve the sample volume and uniform distribution of MNP.

The iron concentration of each sample was determined by photometry using MNP dissolved in hydrochloric acid and stained by PerI's Prussian Blue reaction.

### 2.2. SMF

Magnetic fractionation was performed using a commercially available separation column (MS column, Miltenyi Biotec, Germany). The columns capture bed consists of soft magnetic iron spheres to create local magnetic gradients in an applied magnetic field. To generate small magnetic fields up to 12 mT we used a 10 layer copper coil (200 mm height, 125 windings per layer). For a large field strength of 0.5 T a commercial separator (MiniMACS<sup>™</sup>, Miltenyi Biotec, Germany) was used. Before fractionation the separation column was washed with degassed Triton X-100 solution to prevent clogging and to ensure homogeneous flow conditions.

To separate large magnetic moment MNP 400  $\mu$ L of the sample of initial state were poured onto the column during the presence of a small magnetic field of 12 mT. After collecting the negative fraction the column was gently washed with 200  $\mu$ L of Triton X-100 solution. Subsequently, the magnetic field was decreased down to 1.5 mT and the majority of the captured MNP, fraction M2, were eluted using 200  $\mu$ L of carboxydextran solution. The separation procedure was then repeated with an increased magnetic field strength of 500 mT using the negative fraction of the previous separation. Small magnetic moments not captured by the magnetic force were eluted within the negative fraction M1 (Fig. 1).

### 2.3. A4F

For hydrodynamic size separation of the Resovist<sup>®</sup> particles we used A4F which is based on an elution method where the hydrodynamic diameter  $d_{hyd}$  of an MNP is related to its retention time  $t_r$  within a separation channel with a rectangular cross section, where two perpendicular forces act on MNP. While the longitudinal flow  $V_{Vol}$  carries the MNP through the separation channel, the cross flow  $V_x$  moves the particles towards the bottom of the channel which consists of a semi-permeable ultrafiltration membrane. Due to the smaller diffusion coefficient larger particles are accumulated in an average distance closer to the membrane than smaller particles. Hence, due to the parabolic flow profile of the narrow channel larger particles, moving in slower flow lines, are eluted later (see Fig. 2). This can be approximately described by Giddings equation [15]:

$$t_r = \pi \eta d_{hyd} h \exp(2)/(2k_B T) V_{Vol} / V_x \quad (1)$$

where  $k_B T$  is the thermal energy,  $\eta$  is the viscosity of the carrier liquid,  $d_{hyd}$  is the hydrodynamic diameter of the MNP,  $h$  is the channel height, and  $V_{Vol}$  is the volumetric flow rate through the channel.

The A4F unit (Postnova Analytics GmbH, Germany) consisted of an AF2000 focus system (PN 5200 sample injector, PN 7505 inline degasser, PN 1122 tip and focus pump). As a supplemental feature the A4F unit was equipped with a slot outlet technique for increased sensitivity and elevated concentration of the resulting fractions [10].

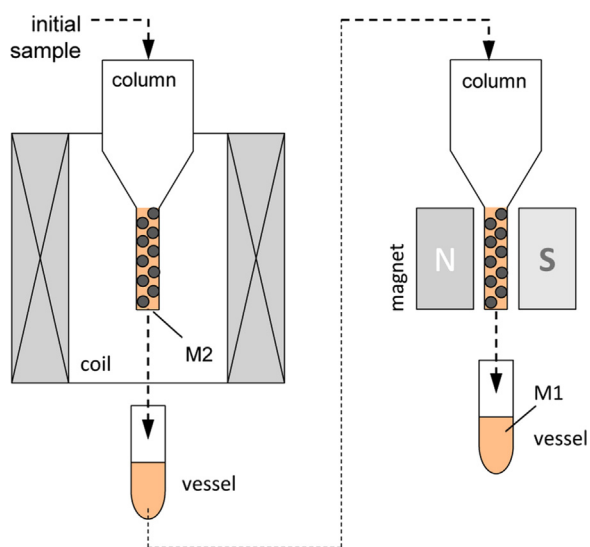


**Fig. 1.** SMF procedure: In the presence of a magnetic field of  $B = 12$  mT (generated by a coil) Resovist<sup>®</sup> was rinsed through a separation column (filled with soft magnetic spheres). The eluted negative fraction was collected for the following separation step. After the magnetic field was decreased down to 1.5 mT the retained MNP of larger magnetic moments were washed out (fraction M2). Subsequently the second separation was performed on the negative fraction of the previous step now in an increased magnetic field of 500 mT. The smallest MNP not attracted were collected (fraction M1).

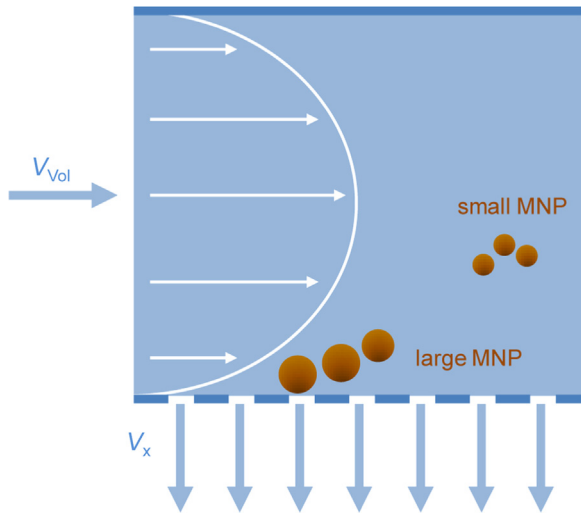


**Fig. 2.** Sketch of the A4F principle: Due to the parabolic flow profile in the channel with flow rate  $V_{Vol}$  a higher flow velocity is reached at the middle of the channel compared to the bottom site. When a cross flow  $V_x$  additionally is applied (through a ultra-filtration membrane) smaller particles accumulate in layers above larger particles and thus elute earlier.

The sample of initial state was further diluted 1:4 in A4F carrier liquid prior to fractionation. We collected 35 fractions at intervals of 1 min in 6 repetitions and accordingly labeled them H1 to H35. The UV detector signal showed two distinct maxima at different elution times which can be attributed to a small and a large sized fraction. Our used setup and fractionation conditions were the same as reported in [4].

The results of the current experiment were in good agreement with previously reported hydrodynamic fractionation of Resovist<sup>®</sup> (using same A4F setup and conditions), as will be detailed in an upcoming publication [4,16]. For reasons of comparison with SMF one small sized fraction with an early elution time of 8 min (H8) was selected for a detailed analysis. Additionally, seven fractions of later elution times corresponding to the larger population H21 to H27 will be more closely examined.

#### 2.4. DLS

For DLS measurements a Malvern Instruments particle sizer (Zetasizer Nano ZS, Malvern Instruments, UK) equipped with a He-Ne laser ( $\lambda=632.8$  nm) was used. Scattering data were recorded in backscattering modus at a scattering angle of  $173^\circ$  at  $T=20^\circ\text{C}$ . The samples were placed into a square  $10 \times 10$  mm disposable polystyrene cuvette. The hydrodynamic diameter,  $d_{hyd}$  (spherical non-interacting particles assumed), was obtained from the diffusion coefficient using the Stokes–Einstein relation,  $d_{hyd}=k_B T/(3\pi\eta D)$  and will be further expressed as the volume-weighted diameter  $d_{DLS}$ .

#### 2.5. MRX

We used a low-Tc-SQUID based MRX device to study the relaxation behavior of our samples [17]. In MRX, the sample is magnetized in a magnetic field of 2 kA/m for 1 s. Then, after switching off the magnet and 500  $\mu\text{s}$  delay, necessary for recovery of the electronics, the magnetization decay of the MNP is recorded by a sensitive SQUID sensor for about 0.5 s at a sample rate of 100 kHz. Note that the range of MNP sizes participating to the MRX signal is limited by the observation window, i.e. MNP having a relaxation time much shorter than the dead time (usually small MNP) have almost decayed before their detection is possible.

With regard to the distinction between core and hydrodynamic properties of the MNP we measured the samples in immobilized and liquid state. The relaxation via Néel mechanism of MNP is measured on immobilized samples to suppress the Brownian relaxation contribution. In this case the relaxation time constant is solely governed by MNP core properties:  $\tau_N=\tau_0\exp(E_A/(k_B T))$  with the prefactor  $\tau_0\sim 10^{-10}$  s [18], and the effective anisotropy energy  $E_A$  (product of effective anisotropy constant  $K_{eff}$ , and the spherical particle core volume  $V_c=\pi d_c^3/6$ ). For the reconstruction of the log-normal size distribution  $f(E_A)$  of the effective anisotropy energy  $E_A$  (with distribution width  $\sigma_{EA}$ ) we used the Moment Superposition Model (MSM) which superimposes the relaxation contributions of non-interacting magnetic moments with different Néel relaxation times [19].

As MNP are dispersed in a carrier fluid Brownian rotation of the MNP may also determine the relaxation of the net magnetization expressed by the time constant:  $\tau_B=3\eta V_{hyd}/(k_B T)$ , where  $\eta$  denotes the dynamic viscosity, and  $V_{hyd}$  the hydrodynamic volume. In this case both relaxation processes are present at the same time and the one with the shortest relaxation time prevails as described by the effective relaxation time:  $\tau_{eff}=\tau_N\tau_B/(\tau_N+\tau_B)$ . For this purpose, we analyzed relaxation curves of liquid samples by fitting the Cluster Moment Superposition Model (CMSM) to measured MRX data. The CMSM superimposes the relaxation contributions of non-interacting MNP and MNP clusters according to their log-normal hydrodynamic size distribution  $f(d_{V,hyd})$  [20].

From  $f(d_{V,hyd})$  we estimated the diameter of the mean volume (here  $d_{V,hyd}$ ) and the dispersion parameter  $\sigma_d$  (logarithm of the geometric standard deviation) representing the relative distribution width of  $d_{V,hyd}$ .

#### 2.6. MPS

The MPI signal was analyzed by means of the spectral response of the samples under investigation using a commercial Magnetic Particle Spectrometer (MPS-3, Bruker, Germany). MPS is a suitable technique for tracer evaluation as it is based on the same physical principle as MPI waiving of any spatial information [21].

Generating a strong AC magnetic field (amplitude  $B_{excit}$  up to 25 mT) with fixed frequency  $f_0$  of 25 kHz the induced magnetization of the MNP was recorded over a 10 s interval by the receiving coils (sensitivity down to  $5 \times 10^{-12}$  Am<sup>2</sup>). The measured signal was filtered to remove the excitation frequency and subsequently amplified. A Fourier transformation of the response results in spectral components showing distinctive amplitudes  $\mu_k$  and phases  $\varphi_k$  at odd multiples of the drive frequency  $k$ . Even harmonics one order of magnitude smaller due to field offset were omitted. In this study all measurements were performed at  $T=295$  K.

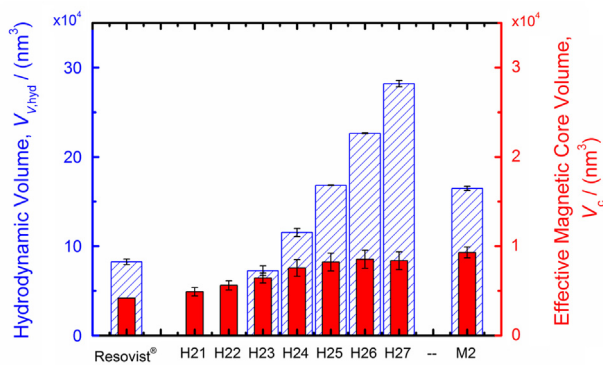
### 3. Results

#### 3.1. Hydrodynamic size

MRX measurements were performed on samples obtained by SMF and A4F in liquid state. Only for fraction H23 to H27 and for M2 MRX signals were observable. The absence of MRX signals for all other samples were attributed to too fast (small MNP) or too slow relaxation times (large MNP) according to the MRX detection interval. Subsequently, we have determined the hydrodynamic size  $d_{V,hyd}$  of M2 (from SMF) and H23 to H27 (from A4F) fitting the above-mentioned CMSM to MRX relaxation curves (see Section 2.5). Using DLS the volume-weighted hydrodynamic size  $d_{DLS}$  could be measured for all fractions. The results are presented in Table 1.

**Table 1**Parameters of Resovist<sup>®</sup> (initial state: IS) and its fractions from A4F and SMF obtained by MRX, DLS and MPS ( $B_{\text{excit}}=25$  mT,  $f_0=25$  kHz).

ID	Hydrodynamic size				Anisotropy		MPI signal change
	$d_{V,\text{hyd}}$ (nm)	$\sigma_d$	$d_{\text{DLS}}$ (nm)	PDI	$E_A/k_B T$	$\sigma_{EA}$	$\mu_3/\mu_{3,IS}$ (%)
IS	54(2)	0.41(1)	43	0.19(1)	7(1)	0.271(2)	100(7)
H8	–	–	12	0.181(3)	–	–	1.7(2)
H21	–	–	44 <sup>a</sup>	0.09(1)	7(1)	0.141(6)	207(15)
H22	–	–	49	0.090(4)	8(1)	0.138(4)	217(15)
H23	52(4)	0.25(2)	56 <sup>a</sup>	0.095(6)	9(1)	0.137(3)	211(15)
H24	60(2)	0.29(1)	63	0.10(1)	11(2)	0.128(2)	205(14)
H25	68.5(1)	0.238(1)	70 <sup>a</sup>	0.098(6)	12(2)	0.145(3)	208(15)
H26	75.6(1)	0.227(2)	76	0.091(6)	13(2)	0.146(4)	209(15)
H27	81(1)	0.209(7)	83 <sup>a</sup>	0.15(2)	12(2)	0.155(5)	199(14)
M1	–	–	10	0.093(1)	–	–	1.5(2)
M2	68(1)	0.38(4)	64	0.251(4)	13.7(9)	0.132(3)	213(15)

<sup>a</sup> The DLS values were obtained by interpolation of DLS data according to [16].

**Fig. 3.** The mean volume of the volume-weighted size distribution of SMF and A4F fractions: The hydrodynamic volume (blue shaded bars) was obtained by fitting the CSM to MRX data. To obtain the effective magnetic core size (red filled bars) the MSM was used with  $K$  fixed at  $6 \text{ kJ/m}^3$ . (For interpretation of the references to color in this figure legend, the reader is referred to the web version of this article.)

A linear increase of the hydrodynamic size from 44 nm up to 89 nm was found for H21 to H27 measured with MRX (Fig. 3) and DLS. The results of both methods were in good agreement. Additionally, the size distribution width  $\sigma_d$  obtained by MRX was about  $\sigma_d=0.24$  for H23 to H27 which is significantly more narrow compared to the initial state ( $\sigma_d=0.41$ ). The size distribution width obtained by DLS (PDI) showed the same trend. The fraction M2 exhibits a hydrodynamic diameter  $d_{V,\text{hyd}}=64$  nm (or  $d_{V,\text{hyd}}=68$  nm from DLS) which is in the size range of H25 (Fig. 3). But more importantly, M2 shows a much broader distribution width  $\sigma_d=0.38$  which is still more narrow compared to the initial state but significantly larger than for the A4F fractions.

In those fractions representing the small size population M1 and H8 we found  $d_{\text{DLS}}=10$  nm and 12 nm, respectively, by DLS (Fig. 3).

### 3.2. Anisotropy

The anisotropy energy  $E_A$  was obtained from fitting the MSM to MRX data measured for immobilized fractions (in Table 1, expressed in  $k_B T$  units with  $T=295$  K). As it can clearly be seen  $E_A/k_B T$  increases from 7 up to 13 for H21 to H25 and then remains constant. For M2 a slightly higher anisotropy energy  $E_A/k_B T=13.7$  was obtained. All fractions except those which showed no MRX signals, exhibit a larger anisotropy energy  $E_A$  compared to the initial state which might be attributed to a larger effective magnetic core size  $d_c$  provided that  $K$  remains constant (Fig. 3).

Then an increase of the effective magnetic core diameter  $d_c$  by 25% will increase  $E_A$  by factor of about 2. For the small size fraction M1 and H8 no MRX signal was observed. We attribute this to the Néel relaxation time falling short of the dead time of our MRX system. Regarding the width of the energy barrier distribution the smallest values were found for M2 and H24 with  $\sigma_{EA}=0.132$  and  $\sigma_{EA}=0.128$ , respectively. For the sample of initial state a twice as broad distribution  $\sigma_{EA}=0.271$  was found.

### 3.3. MPS

All measured MPS amplitude spectra were normalized to the sample's respective iron amount (Fig. 4). For A4F fractions a higher MPS amplitude  $\mu_3$  was found for later elution times. Regarding the small sized fractions M1 (from SMF) and H8 (from A4F)  $\mu_3$  reached only 2% compared to the sample of initial state and a significantly steeper decline of the h74armonic amplitudes  $\mu_k$ . Furthermore, the phase  $\varphi_3$  of the small sized fractions is considerably larger than for native Resovist<sup>®</sup> and  $\varphi_k$  decreases linear with increasing harmonic number  $k$ .

The MPS amplitudes of the larger fractions H21 to H27 increased up to a maximum of  $\mu_3=0.91 \text{ Am}^2/\text{mol}(\text{Fe})$  (H22,  $d_{\text{hyd}}=49$  nm) which is a factor of 2.2 higher compared to unfractionated Resovist<sup>®</sup>. For H23 to H27  $\mu_3$  slightly decreased. The large fraction M2 from SMF increased also by factor of 2.1.

Regarding the shape of the spectra H22 has a slightly slower decay of the harmonic amplitudes compared to all other larger MNP containing samples. More obviously M2 shows the lowest third harmonic phase  $\varphi_3 = -35.5^\circ$  of the MPS signal and exhibits a pronounced minimum at  $k=11$ . Also for H22 the overall phase is lower compared to the sample of initial state (Fig. 4).

## 4. Discussion

A4F and SMF carried out on Resovist<sup>®</sup> verified the presence of a broad hydrodynamic size and anisotropy energy distribution as reported earlier [4,9]. For A4F the hydrodynamic size and anisotropy energy are not correlated linearly. This might be attributed to a size dependence of the multi-core structure (e.g. packing density of single cores) because  $E_A$  of such clusters is determined by single core properties as well as dipole–dipole-interactions between them [22]. The large sized fraction produced by SMF has a broader hydrodynamic size distribution and larger anisotropy energy  $E_A$  compared to all other fractions obtained by A4F. This may be due to the fact that the SMF does not hydrodynamically distinguish between MNP sizes and the used separation fields are not

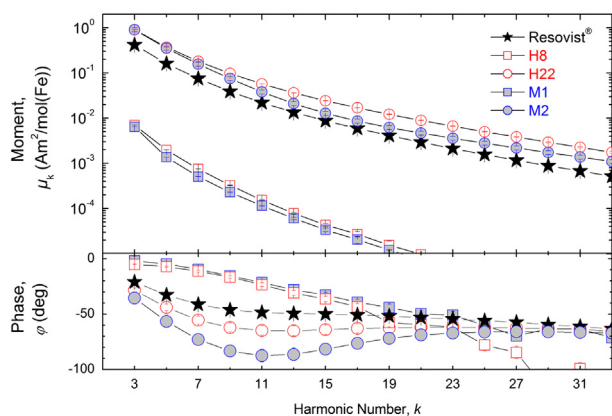


**Fig. 4.** MPS measurement ( $B_{\text{excit}}=25$  mT,  $f_0=25$  kHz): MPS spectra  $\mu_k$  measured on fractions from SMF and A4F (top diagram) and the related phase lag  $\varphi_k$  (bottom diagram). The spectra of the small fractions (squares) both have 100-fold weaker signal amplitudes compared to the initial state, whereas the third harmonic amplitude  $\mu_3$  of the large fractions (circles) yield a gain of factor 2.2. For higher harmonic amplitudes the performance of the larger A4F fraction is slightly better. Interestingly the phase lag of the larger fractions is very different and indicates the presence of larger hard magnetic components in the SMF fraction.

strictly selective. However, the observed structural difference did not affect the MPS amplitude of M2 as the third harmonic amplitude  $\mu_3$  increased up to 220% for both methods. The structural differences of SMF and A4F fractions H22 and M2 are reflected more obviously in the phase of the MPS signal. For M2 the phase exhibits a pronounced minimum which may indicate the presence of magnetically harder components which is in good agreement with  $E_A$  values. This finding seems to support the idea about the difference in separation mechanism. Thus, in SMF the column retains particularly the MNP with larger and less thermally fluctuating (Néel) magnetic moments, whilst A4F selects only by size.

Furthermore, the MPS amplitude of small MNP was 150-fold lower than for larger MNP because these weak magnetic moments need higher drive fields to enter the nonlinear part of their magnetization curve. The phase lag was found to be near zero which is in good agreement with the fast Néel relaxation time as discussed in 3.1.

## 5. Conclusion

We demonstrated the potential of improving MPI performance of MNP present in Resovist<sup>®</sup> by two different fractionation methods. It is obvious, that both methods result in fractions of MNP where the relation between physical and magnetic structure differs. A4F was shown to produce narrow hydrodynamic size classes and is an excellent tool for the hydrodynamic characterization of MNP. In contrast, SMF may produce a broader distribution of hydrodynamic sizes. With respect to the MPI performance of Resovist<sup>®</sup> SMF yields a similar improvement for MPI. It has the practical advantage that the resulting fractions are not highly diluted as after A4F and can be directly used for further experiments. These results are a step forward towards understanding MPI performance of Resovist<sup>®</sup> which is important to design novel MPI tracer and could help for further developments of separation techniques.

## Acknowledgment

This research was financially supported by German Research Foundation, through DFG Research Unit FOR917 Nanoguide (Grant TR408/-1) and KFO213 (Grant TR408/5-2).

## References

- [1] B. Gleich, J. Weizenecker, Tomographic imaging using the nonlinear response of magnetic particles, *Nature* 435 (2005) 1214–1217.
- [2] R.M. Ferguson, K.R. Minard, K.M. Krishnan, Optimization of nanoparticle core size for magnetic particle imaging, *J. Magn. Magn. Mater.* 321 (2009) 1548–1551.
- [3] J. Weizenecker, B. Gleich, J. Rahmer, J. Borgert, Micro-magnetic simulation study on the magnetic particle imaging performance of anisotropic monodomain particles, *Phys. Med. Biol.* 57 (2012) 7317.
- [4] A.F. Thünemann, S. Rolf, P. Knappe, S. Weidner, In situ analysis of a bimodal size distribution of superparamagnetic nanoparticles, *Anal. Chem.* 81 (2009) 296–301.
- [5] E. Romanus, T. Koettig, G. Glöckl, S. Prass, F. Schmidl, J. Heinrich, P. Seidel, Energy barrier distributions of maghemite nanoparticles, *Nanotechnology* 18 (2007) 115709.
- [6] T. Rheinländer, R. Kötz, W. Weitschies, W. Semmler, Magnetic fractionation of magnetic fluids, *J. Magn. Magn. Mater.* 219 (2000) 219–228.
- [7] N. Löwa, D. Eberbeck, U. Steinhoff, F. Wiekhorst, L. Trahms, Potential of improving MPI performance by magnetic separation, in: T.M. Buzug, J. Borgert (Eds.), *Magnetic Particle Imaging*, Springer, Berlin Heidelberg, 2012, pp. 73–78.
- [8] F. Ludwig, T. Wawrzik, T. Yoshida, N. Gehrke, A. Briel, D. Eberbeck, M. Schilling, Optimization of magnetic nanoparticles for magnetic particle imaging, *IEEE Trans. Magn.* 48 (2012) 3780–3783.
- [9] T. Yoshida, N.B. Othman, K. Enpuku, Characterization of magnetically fractionated magnetic nanoparticles for magnetic particle imaging, *J. Appl. Phys.* 114 (2013) 173908.
- [10] P. Knappe, A4F-SAXS Online-coupling for the Investigation of Nanoparticles and Polymers, Dissertation, 2012.
- [11] J. Lohrke, A. Briel, K. Mäder, Characterization of superparamagnetic iron oxide nanoparticles by asymmetrical flow-field-flow-fractionation, *Nanomedicine* 3 (2008) 437–452.
- [12] S. Dutz, J. Kuntsche, D. Eberbeck, R. Müller, M. Zeisberger, Asymmetric flow field-flow fractionation of superferromagnetic iron oxide multicore nanoparticles, *Nanotechnology* 23 (2012) 355701.
- [13] R.M. Ferguson, A.P. Khandhar, K.M. Krishnan, Tracer design for magnetic particle imaging (invited), *J. Appl. Phys.* 111 (2012) (7B318–317B3185).
- [14] R. Lawaczeck, M. Menzel, H. Pietsch, Superparamagnetic iron oxide particles: contrast media for magnetic resonance imaging, *Appl. Organomet. Chem.* 18 (2004) 506–513.
- [15] J.C. Giddings, Field-flow fractionation: analysis of macromolecular, colloidal, and particulate materials, *Science* 260 (1993) 1456–1465.
- [16] N. Löwa, P. Knappe, F. Wiekhorst, D. Eberbeck, A.F. Thünemann, L. Trahms, How hydrodynamic fractionation influences MPI performance of resovist<sup>®</sup>, *IEEE Trans. Magn.* <http://dx.doi.org/10.1109/TMAG.2014.2326833> [in press].
- [17] H. Matz, D. Drung, S. Hartwig, H. Groß, R. Kötz, W. Müller, A. Vass, W. Weitschies, L. Trahms, A SQUID measurement system for immunoassays, *Appl. Supercond.* 6 (1999) 577–583.
- [18] L. Bessais, L. Ben Jaffel, J.L. Dormann, Relaxation time of fine magnetic particles in uniaxial symmetry, *Phys. Rev. B: Condens. Matter* 45 (1992) 7805–7815.
- [19] D. Eberbeck, S. Hartwig, U. Steinhoff, L. Trahms, Description of the magnetisation decay in ferrofluids with a narrow particle size distribution, *Magnetohydrodynamics* 39 (2003) 77–83.
- [20] D. Eberbeck, F. Wiekhorst, U. Steinhoff, L. Trahms, Aggregation behaviour of magnetic nanoparticle suspensions investigated by magnetorelaxometry, *J. Phys.: Condens. Matter* 18 (2006) S2829.
- [21] S. Biederer, T. Knopp, T.F. Sattel, K. Lüttke-Buzug, B. Gleich, J. Weizenecker T.M. Buzug, Magnetization response spectroscopy of superparamagnetic nanoparticles for magnetic particle imaging, *J. Phys. D: Appl. Phys.* 42 (2009) 205007.
- [22] V. Schaller, G. Wahnström, A. Sanz-Velasco, S. Gustafsson, E. Olsson, P. Enoksson, C. Johansson, Effective magnetic moment of magnetic multicore nanoparticles, *Phys. Rev. B: Condens. Matter* 80 (2009) 092406.